**Aalborg Universitet**

AALBORG UNIVERSITY
DENMARK

**A lightweight CORONA-NET for COVID-19 detection in X-ray images**

Hadi, Muhammad Usman; Qureshi, Rizwan; Ahmed, Ayesha; Iftikhar, Nadeem

*Published in:*
Expert Systems with Applications

*DOI (link to publication from Publisher):*
[10.1016/j.eswa.2023.120023](https://doi.org/10.1016/j.eswa.2023.120023)

*Creative Commons License*
CC BY 4.0

*Publication date:*
2023

*Document Version*
Publisher's PDF, also known as Version of record

[Link to publication from Aalborg University](https://vbn.aau.dk)

*Citation for published version (APA):*
Hadi, M. U., Qureshi, R., Ahmed, A., & Iftikhar, N. (2023). A lightweight CORONA-NET for COVID-19 detection in X-ray images. *Expert Systems with Applications*, *225*, Article 120023. Advance online publication. https://doi.org/10.1016/j.eswa.2023.120023
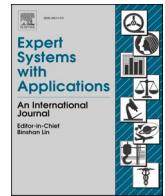
# A lightweight CORONA-NET for COVID-19 detection in X-ray images

Muhammad Usman Hadi [a,*], Rizwan Qureshi [b], Ayesha Ahmed [c], Nadeem Iftikhar [d]

[a] Nanotechnology and Integrated Bio-Engineering Centre (NIBEC), School of Engineering, Ulster University, BT15 1AP Belfast, UK
[b] Department of Imaging Physics, MD Anderson Cancer Center, The University of Texas, Houston, TX 77030, USA
[c] Department of Radiology, Aalborg University Hospital, Aalborg 9000, Denmark
[d] University College of Northern Denmark, Aalborg 9200, Denmark

A B S T R A C T

Since December 2019, COVID-19 has posed the most serious threat to living beings. With the advancement of vaccination programs around the globe, the need to quickly diagnose COVID-19 in general with little logistics is fore important. As a consequence, the fastest diagnostic option to stop COVID-19 from spreading, especially among senior patients, should be the development of an automated detection system. This study aims to provide a lightweight deep learning method that incorporates a convolutional neural network (CNN), discrete wavelet transform (DWT), and a long short-term memory (LSTM), called CORONA-NET for diagnosing COVID-19 from chest X-ray images. In this system, deep feature extraction is performed by CNN, the feature vector is reduced yet strengthened by DWT, and the extracted feature is detected by LSTM for prediction. The dataset included 3000 X-rays, 1000 of which were COVID-19 obtained locally. Within minutes of the test, the proposed test platform's prototype can accurately detect COVID-19 patients. The proposed method achieves state-of-the-art performance in comparison with the existing deep learning methods. We hope that the suggested method will hasten clinical diagnosis and may be used for patients in remote areas where clinical labs are not easily accessible due to a lack of resources, location, or other factors.

## 1. Introduction

SARS-CoV-2 Coronavirus illness, commonly referred to as COVID-19, posed significant problems to the globe since early 2020 and was declared a Pandemic on 12 March by WHO (World Health Organization) (WHO, 2021). It is extremely contagious, that spreads similar to SARS-COV-1, through direct physical contact or indirect contact by aerosolized SARS-COV-2. The (WHO) reports that Wuhan, China, saw the first COVID-19 case in late December 2019. All portions of the planet were affected by early February 2020, and there were strict regulations in place. It has been considered one of the greatest health challenges of the twenty-first century (Giri et al., 2021).

COVID-19 targets the immune system and infects the human body's primary respiratory tract. Evidence suggests that COVID-19 patients have one or more of the symptoms, including coughing, fever, taste and smell loss, exhaustion, weariness, diarrhoea, and illness (Vandenberg, Martiny, Rochas, van Belkum, & Kozlakidis, 2021). From the third to the eighth day, the major symptoms that COVID-19 patients have include difficulty in breathing and a decrease in oxygen saturation. Like COVID-

19 individuals, renal and cardiac problems have been reported (Sisti et al., 2021). More than 683 million of people have confirmed causes of COVID-19 detection while approximately 6.8 million died throughout the world because of ineffective and time-consuming diagnostic examinations (Worldometer, 2023). The world has realized that we must take certain precautions and measures to protect ourselves from these problems.

To tackle this deadly virus, major pharmaceutical firms have made early progress in creating COVID-19 vaccines, and several countries have already immunised their populations. It has been shown that vaccination merely increases the immune system's ability to fight off infection; it does not provide 100 percent protection against the COVID-19 virus.

It will take some time to create a broad-spectrum vaccination that can protect against all COVID-19 variants, but research on vaccines is already ongoing. However, in the fight to end the pandemic, early diagnosis of infection is critical. We are fighting not just this terrible infection, but also the passage of time. COVID-19 can be detected using gene sequencing utilizing the Reverse Transcription Polymerase Chain

Reaction (RT-PCR) approach (Sahajpal et al., 2020). This procedure takes between 8 and 12 h, leaving the pa-tient anxious and unsure of whether they have contracted an infection. Furthermore, the detection accuracy of PCR in the first three days after exposure to COVID is low (Jung et al., 2021; Schuit et al., 2021). According to the research, oropharyngeal swabs and sputum might help discover COVID patients earlier. Nonetheless, the method's biggest drawbacks include handling enormous populations, expenses, and equipment.

Early identification of COVID-19 will increase the COVID patient's life expectancy and allow practitioners to make better judgments and plans. Based on this, the primary focus of research has been on using optical technologies and sensors for early COVID-19 detection.

Over the last year and a half, new approaches for detecting COVID-19 have become increasingly popular. We utilised the terms "detection," "diagnostic," "COVID-19," and "Corona Virus" as searched items in current literature from the web of sciences. The diagnosis of COVID-19 infection may be made by the detection of viral nucleic acid and antigen (acute infection), as well as the detection of antiviral antibodies (pre-infection). Despite the heated discussion over whether antibody-detection assays are suitable or inappropriate, there is still a demand for cutting-edge testing with high sensitivity, specificity, and cost-effective technology.

We proposed a deep learning-based architecture to detect COVID-19, particularly in the age group of 50 to 70 years. The contributions of this article are as follows:

1. A hybrid model consisting of a Convolutional Neural Network (CNN), Discrete Wavelet Transform (DWT), and Long Short-Term Memory (LSTM) network that can automatically help with COVID-19 patient early identification.
2. Using chest X-rays, a dataset of 3000 images was collected from a local hospital in Denmark to detect COVID-19.
3. The proposed system performance is presented in terms of a confusion matrix, accuracy, sensitivity, specificity, and F1-score and it achieves state-of-the-art performance.
4. A statistical analysis of the data is provided to help understand the cycle or map that is followed for COVID-19 detection in the hospital as contrasted to the cycle of activities required in the proposed detection.
5. To test the strategy, it is essential to check that the proposed method recognises COVID-19 and not simply any random object. The sample in this research consisted of COVID-19 patients who visited the hospital citing respiratory problems.

The paper is structured as follows: Section 2 describes the emergence and characteristics of COVID-19 in depth, making the COVID-19 life cycle easier to comprehend. The primary work/literature review that is used to detect COVID-19 is summarized in Section 3. Section 4 discusses the data collection and description of the data followed by Section 5 describes the proposed deep learning CORONA-NET architecture. Section 6 describes the experimental setup and summarizes the findings and results analysis. Section 7 presents the validation of the proposed technique, which includes a comparison of the suggested and radiologist findings while Section 8 presents the limitations of the x-ray based COVID-19 detection and the proposed method. Finally, Section 9 presents the conclusions.

## 2. COVID-19's emergence and characteristics

The genus of viruses known as coronaviruses is responsible for devastating respiratory illnesses. Two zoonotic-coronaviral high pathogens, SARS and MERS, created a deadly respiratory illness in humans in 2012, creating a new danger to public health in the twenty-first century. Concerns about coronavirus evolution have been raised in the field of public health (Mousavizadeh & Ghasemi, 2021; Oberfeld et al., 2020; Yang, Li, Sun, Zhao, & Tang, 2020; Zhu, Zhang, Wang, Li, Yang, Song, & Tan, 2020). In late December 2019, in Wuhan, Hubei Province, China, several medical institutions saw large numbers of pneumonia cases (Taha, Al Mashhadany, Hafiz Mokhtar, Dzulkefly Bin Zan, & Arsad, 2020). Coronaviruses are divided into four genera: Alpha coronavirus, Beta coronavirus, Gamma coronavirus, and Delta coronavirus (Mousavizadeh & Ghasemi, 2021). A novel variation known as B.1.1.529, also called the Omicron variant, was found in South Africa in November 2021. It's been less than a month since scientists in Botswana and South Africa issued an international warning about Omicron, a rapidly spreading SARS-CoV-2 strain. Researchers from all around the world are scrambling to understand the global impact of the mutation, which has now been confirmed in more than 20 countries. It might take weeks for researchers to learn more about Omicron, including its severity and propensity to resist immunizations as well as reinfect people. Omicron patients must have their genomes sequenced to be identified, however, some PCR methods can reveal a distinctive feature of the variation that sets it apart from the Delta variant. The fight against SARS-CoV-2 has grown more challenging after the emergence of Omicron. The Spike protein has undergone several mutations that raise the possibility that the immune protection brought on by the current COVID-19 infection and vaccinations has altered.

An RNA virus with an envelope is the coronavirus. The virus seems to have a halo (Corona) of enormous club-shaped spikes on its surface under a microscope. Through these spikes, the virus may enter cells and begin replicating there after entering the human respiratory system. Respiratory aerosols are the main way that coronavirus spreads. Inhaling aerosols or coming into close contact with the eyes, nose, or mouth may potentially spread the virus. COVID-19 has a 2–10 day incubation period, which is the duration between infection and symptom emergence after being exposed to the virus. However, it can take up to 14 days. Some sick people could be infectious during this stage, which is also frequently referred to as the "pre-symptomatic" phase. As a result, transmission from a disease that is pre-symptomatic may happen before symptoms manifest. Spikes on the virus surface adhere to the cell membrane. The Angiotensin Converting Enzyme-2 functions as a viral receptor in the lower respiratory tract. Typically, the virus only affects the mucosal cells of the respiratory tract. After breaching its envelope, the virus enters the cell and multiplies in the cytoplasm. The endoplasmic reticulum of the cell provides the virus with its envelope once it has replicated. The virus exits the cell when replication is complete and travels to other cells. An important part of the body's Renin-Angiotensin-Aldosterone system, which regulates fluid balance, is the Angiotensin Converting Enzyme-2 (ACE-2). Coronavirus binding to ACE-2 disrupts the body's fluid balance, resulting in diffuse edema of the respiratory tract and hypoxia. Coryza (rhinorrhea), throat irritation, and low-grade fever are symptoms indicating upper respiratory tract involvement. When the lower respiratory tract is affected, pneumonia develops. Severe respiratory distress, fever, a dry cough, dyspnea, and hypoxia are all signs of pneumonia.

Spike (S), membrane (M), envelope (E), and nucleocapsid (N) are the four separate components of the virus. Of all known RNA viruses, it possesses the biggest genome (26.4–31.7 kb). Single-stranded RNA is also included in the genetic makeup of the virus (Antiochia, 2020; Feng et al., 2020; Passaro et al., 2012) The COVID-19 structure is shown in Fig. 1.

COVID-19's lifecycle is depicted in Fig. 2 below. Physical contact, sneezing, coughing, and inhaling droplets are common ways for HPV to spread from the host. These droplets have the potential to enter the respiratory tract.

## 3. Literature review

An overview of the diagnostic approaches in the recent past is presented in the next section (2020–21). We searched the web of sciences for recently published material on the phrases "COVID-19 Detection" and "Methods to Detect COVID-19." As demonstrated in Fig. 3, we were
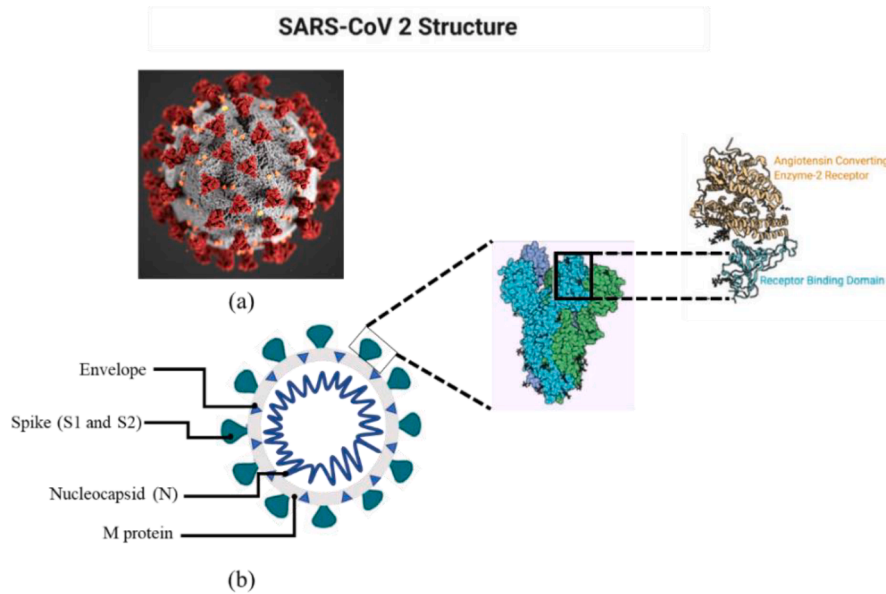
**Fig. 1.** SARS-CoV2 is depicted in (a) as a microscopic picture and (b) as a structural diagram. SARS-CoV-2 structural diagram displaying the spikes, envelope, nucleocapsid, and M protein. The spike's structure is seen in the inset. Shows the microscopic image of SARS-CoV2 while (b) shows the structural diagram of SARS-CoV2. Structural schema of SARS-CoV-2 showing Spikes, envelope, nucleocapsid and M protein. The inset shows the structure of the spike.
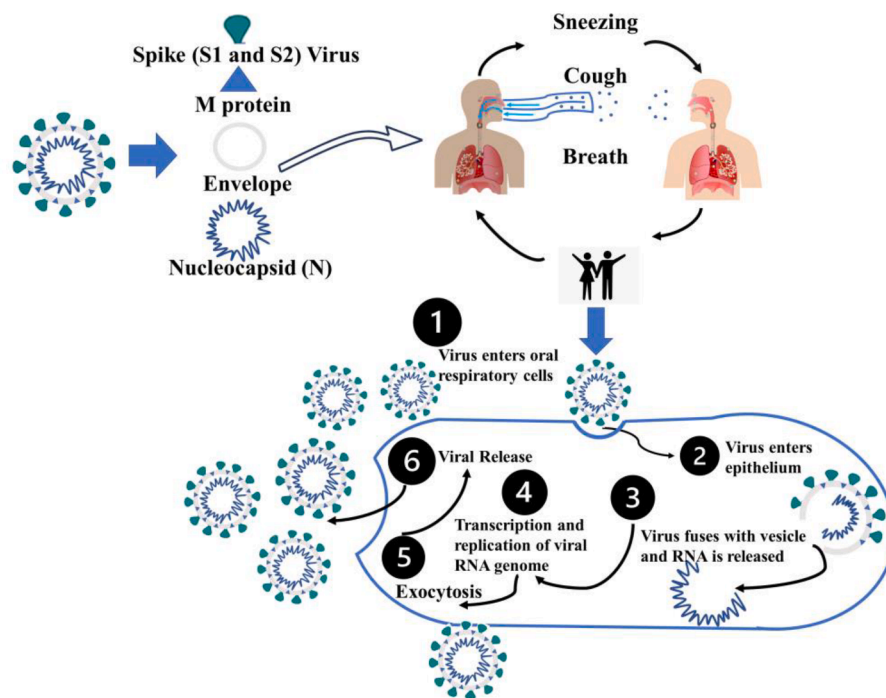


**Fig. 2.** SARS-cycle CoV-2′s of infection (COVID-19). The procedures involved in the transmission and replication of the Coronavirus are outlined in the life cycle.

able to get the following cluster, which displays the methodologies used for COVID-19 detection.

Many scholars used artificial intelligence algorithms to address medical difficulties in recent years. Deep learning algorithms are being applied in a variety of applications (Kallianos et al., 2019; Wang, Wang, & Zhang, 2018; Zhang, Wang, Li, & Han, 2018). Convolution Neural Networks (CNNs) are normally used for analyzing medical images; including the segmentation of brain tumours, the detection of breast cancer, and the categorization of lung diseases in X-ray pictures, among other things. Computer Scientists have already developed several ways

for illness identification from biomedical imaging data. Sharma and Miglani (2020) presents a survey with potential solutions and future issues of medical image processing. Lee & Fujita (2020) outline many research that used deep learning algorithms to diagnose a variety of disorders. Cho et al. (2020) used a deep convolution neural network to propose a strategy for dermatologist-level categorization of malignant lip disorders. The author used a collection of 1629 clinical pictures to train the ResNet model.

Deep transfer learning techniques were used to precisely diagnose pneumonia in chest X-ray pictures (Hashmi, Katiyar, Keskar, Bokde, &
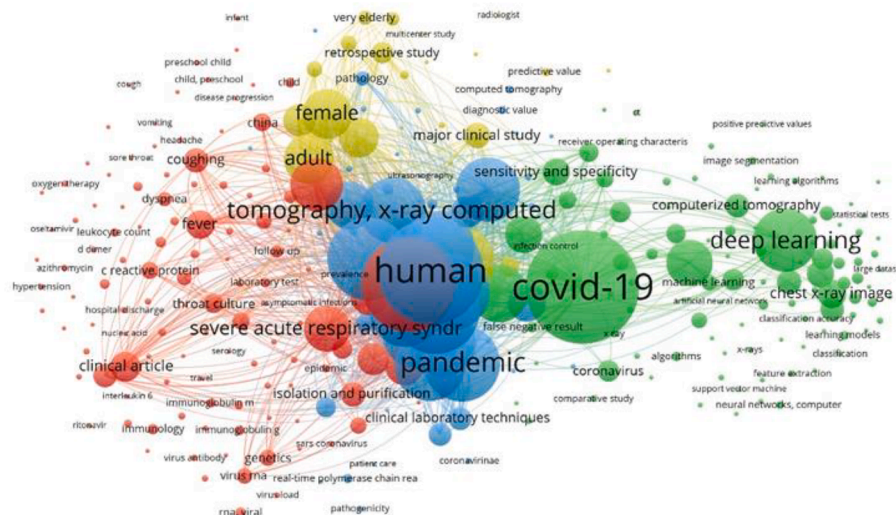
**Fig. 3.** Cluster for the search items for COVID-19 detection from the web of sciences.

Geem, 2020). A weighted classifier-based ensemble technique is illustrated. The suggested model blends cutting-edge deep learning techniques with the predictions of a weighted classifier to generate a new model. Son et al. (2020) proposed a deep learning method for identifying different flaws in retinal fundus pictures. Similarly, Baltruschat, Nickisch, Grass, Knopp, and Saalbach (2019) proposed a comparison of deep learning algorithms for multi-label chest X-ray classification where transfer learning is used in this work both with and without fine-tuning.

Nasrullah et al. (2019) came up with a new method based on a pair of custom-designed three-dimensional mixed links categorization and detection of lung cancer using networks (CMixNet) cancer. A gradient was used to categorise lung nodules using extracted features from the boosting machine (GBM) CMixNet is a module that allows it to connect to other computers through the internet. Several parameters were used to compare the outcomes of deep learning nodule-based classification; such as the patient's family history, smoking history, age, and so on. Yao, Poblenz, Dagunts, Covington, Bernard, and Lyman (2017) simulated the long short-term memory network and DenseNet to extract anomalies and dependencies. In this article, the authors proposed a two-stage end-to-end neural network approach, combining a densely connected image encoder with a recurrent neural network decoder.

Khatri, Jain, Vashista, Mittal, Ranjan, and Janardhanan (2020) proposed that non-infected and infected lungs be classified using the earth movers' distance (EMD) algorithm. Pre-processing is carried out on the raw images to exclude any non-lung regions. After that, the preprocessed image is scaled and normalised by intensity to provide a set of homogeneous lung shapes and sizes. Stephen, Sain, Maduh, and Jeong (2019) proposed a deep learning strategy for pneumonia classification that is both efficient and effective. A CNN model is used in this study for the identification and classification of pneumonia using chest X-rays. The most important COVID-19 detection methods and approaches are addressed in Table 1 in terms of, specifics, effectiveness, benefits, and drawbacks.

## 4. Dataset collection and description

The whole method for detecting COVID-19 consists of numerous steps as depicted in Fig. 4 (a). The preprocessing pipeline was used to send raw X-ray images that consist of data resizing followed by shuffling and normalization. The dataset is divided into training, validation and testing subsets. We used the validation data to fine-tune the hyperparameters. Confusion matrix, accuracy, specificity, sensitivity,

precision, and F1-score are used as performance metrics.

For the preparation of the data, first, we chose 130 X-rays from each of the COVID-19 patients and viral pneumonia cases at Aalborg Hospital (AH), Aalborg, Denmark. We gathered 870 X-ray images of COVID-19 patients using Radiopaedia (Bell et al., 2023), The Cancer Imaging Archive (TCIA) (Clark et al., 2013), and the Italian Society of Radiology (SIRM) (SIRM COVID-19, 2021). We used the Kaggle repository (Mooney, 2018) and the NIH dataset (NIH, Kaggle, 2021) to collect 870 X-rays of viral pneumonia patients and 870 X-ray images of normal cases. The resolution of X-ray images is $256 \times 256$ while the partitioning of the data set is shown in Table 2. Fig. 4 (b) shows the images of Normal, COVID-19 and Viral Pneumonia X-rays.

## 5. CORONA-net architecture

The proposed network consists of the following components:

  (i) CNN (Spatial Feature extractor / backbone-model).
 (ii) DWT (Feature Detector).
(iii) LSTM (Temporal feature detector).
(iv) Dense layer (Classification head).

### Convolutional neural network

A CNN extracts the features in a hierarchical pattern, typically used for images or the data which lies in the form of a grid. In numerous applications such as image classification, object identification, and medical image analysis, CNNs have demonstrated excellent performance (Alzubaidi et al., 2021). The fundamental idea behind a CNN is that it can take local characteristics from inputs at high levels and transfer them to lower layers for more complex feature learning. Convolutional, pooling, and fully linked layers make up a CNN. A typical CNN configuration with these layers is shown in Fig. 5.

### Convolution layer

A CNN's initial layer is the convolutional layer. It extracts features from an input image by performing the convolution and generates a feature map using a kernel (convoluted image). The dimension of the feature map is further reduced by max or average pooling operation. The kernel size and the number of kernels are hyperparameters.

### Kernel

A real-valued matrix with a small n connection to the input matrix makes up the kernel (input picture). By extracting a patch from the input image that fits inside the kernel dimension and performing a dot

**Table 1**

Diagnostic techniques to detect SARS-CoV-2.

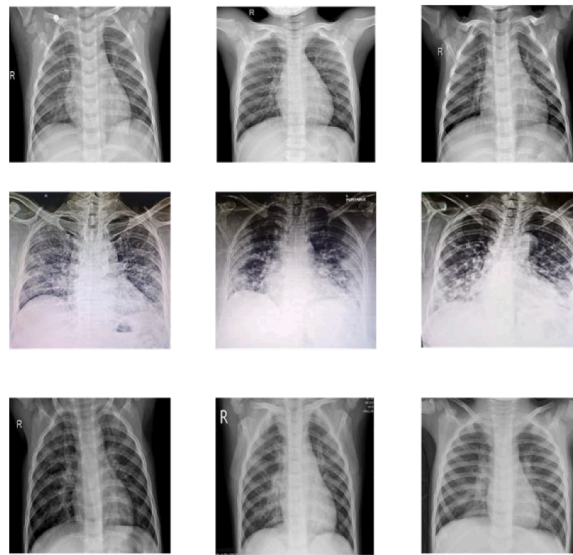| No. | Type | Details | Efficiency ($\eta$) | Pros | Cons |
|---|---|---|---|---|---|
| 1 | Polymerase Chain Reaction (PCR) Test | The testing technique involves the following steps: (i) specimen collection; (ii) clinical specimen packaging (storage) and transportation; (iii) (good) communication with the laboratory and giving the necessary information; (iv) laboratory testing; and (v) reporting the results (Kakodkar, Kaka, & Baig, 2020). | The time it takes to get the results can be as long as two or three days. Only 66 to 80% of it is sensitive (Cai et al., 2020). | The RT-PCR technique necessitates expensive laboratory equipment, which is frequently found in a central laboratory (biosafety level 2 or higher). As a result, the outcome is extremely dependable. | Commercial PCR-based procedures are costly and reliant on technical knowledge, and the presence of viral RNA or DNA does not always indicate acute illness. |
| 2 | IgM / IgG Rapid Test | Immunoassays are tests that detect particular antibodies in the blood of a patient. A 15-minute lateral flow immunoassay has been developed to detect IgM and IgG in human blood. | COVID-19 IgM / IgG Rapid Test Sensitivity is 88.66% | Employing a synthetic peptide as an antigen improves the immunoassay's stability and reproducibility and is theoretically more specific than using a virus as an antigen. | Typically, the immunoassay yields only qualitative results. |
| 3 | A disease diagnosis model based on radio and clinical characteristics (Nguyen, Duong Bang, & Wolff, 2020). | Only CT imaging and clinical symptoms can distinguish between pneumonia patients with and without COVID-19. These models will be crucial for quick and straightforward diagnosis, especially when RT-PCT kits and experimental platforms for COVID-19 infection screening are in low supply (Nguyen et al., 2020). | In primary and cohort validation, the area under the curve was 0.986 (95 percent confidence interval 0.966 1.000) and 0.936 (95 percent confidence interval 0.866 1.000), respectively (Kakodkar et al., 2020). | The clinical and radiological semantic models performed better in terms of diagnostic accuracy and yielded greater net benefits. | According to the study, 18 radiological and 17 clinical characteristics were determined to be relevant in forming COVID-19 infection predictions. |
| 4 | (Loop-mediated isothermal amplification) LAMP assay | This approach uses a set of four specially designed primers and a DNA polymerase with strand displacement activity. Instead of heat denaturation, LAMP generates a singlestranded template using stranddisplacement polymerase (Chen et al., 2020) | At a steady temperature of 65 °C, LAMP can manufacture up to 109 copies of target DNA in less than an hour. Detection sensitivity is greater than 95%. | LAMP has a good sensitivity and is simple to execute, but it also has the potential to run at a fixed temperature, which reduces the phenomenon affects of a thermocycler while also reducing the amount of energy used. | The LAMP technique's clinical usefulness for SARS-CoV-2 has yet to be investigate |
| 5 | Luminescent Immunoassay | Luminescent immunoassays are approaches for lowering the detection limits of antibody-based reagents. Chemiluminescence and fluorescence are commonly used (Nguyen, 2020) | IgG was found in 71.4 percent of all sera (197/276), which is 192 percent greater than IgM (57.2 percent, 158/276). The detected rate was increased to 81.5 percent (225/276) when the two 193 antibodies were combined. In SARS, different sensitivity of the 194 IgG and IgM detection techniques have been recorded. | Diazyme Laboratories Inc. has revealed details of two new fully automated SARS-CoV-2 serological assays that can be done on the Diazyme DZ-lite 3000 Plus chemiluminescence analyzer. | It is currently approved for usage in the United States, China, and Brazil |
| 6 | Biosensing Method | Biosensor tests rely on optical, electrical, enzymatic, and other techniques to translate the unique activity of biomolecules into a quantitative output (Maghdid et al., 2021) | Within 10 min, the surface plasmon resonance (SPR) chip detected anti-SCVme antibodies at a lower limit of detection of 200 ng/mL. | PathSensors Inc. recently developed a CANARY biosensor to detect the new SARS coronavirus. This approach makes use of a cell-based immunosensor that combines viral collection with signal amplification to produce a result in 35 min. | In May 2021, the biosensor will be available for research purposes. |
| 7 | X-ray images (Maghdid et al., 2021) | X-ray-based AI system | Detection is around 89% | Early detection and no need of waiting as required in terms of PCR test method. | Medical Training and Physician still required to approve the diagnosis. |
| 8 | X-ray imaging (Ozturk et al., 2020) | Bayesian Convolutional Neural Network based detection | Detection is around 91% | Early detection and no need of waiting as required in terms of PCR test method. | Medical Training and Physician still required to approve the diagnosis. |
| 9 | X-ray imaging (Nguyen, Cai, & Chu, 2019) | Res-Net based detection AI system | Detection is around 96% | Early detection and no need of waiting as required in terms of PCR test method. | Learning parameters are excessively complex, and include gradually modifying the size, looping the learning rate search, and discerning the learning rate. |
| 10 | X-ray imaging (Nguyen et al., 2019) | Bayesian Convolutional Neural Network based detection | Detection is around 91% | Early detection and no need of waiting as required in terms of PCR test method. | Medical Training and Physician still required to approve the diagnosis. |
| 11. | CXR images | Transfer learning (Loey, Smarandache, & Khalifa, 2020) | NA | Minimize the false positive rate. | It still ignores the spatial relationship. |
| 12. | CXR images | VGG-16 (Civit-Masot, Luna-Perejón, Domínguez Morales, & Civit, 2020) | NA | Popular in CXR image analysis. | Over-fitting problem. |
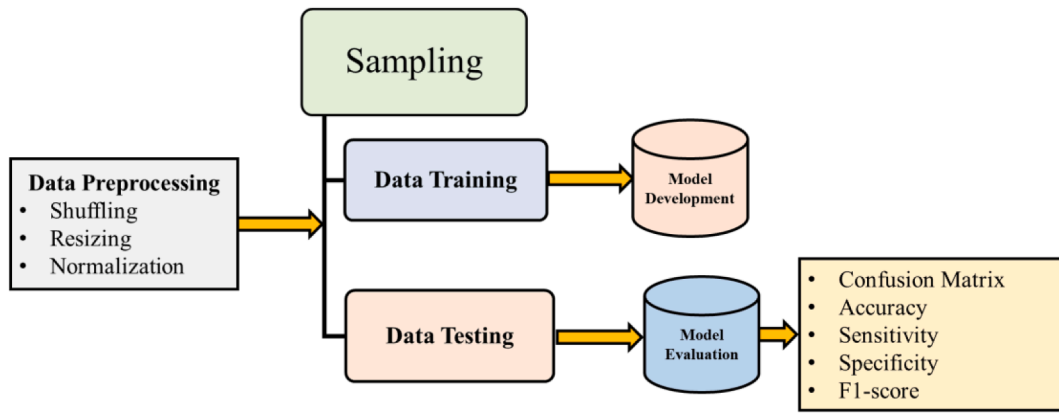
(a)



(b)

**Fig. 4.** (a) Block diagram of the proposed CORONA-NET detection system, (b) and the X-ray images in the first, second, and third rows showing three sample images of Normal, COVID-19 and pneumonia specimens respectively.

**Table 2**
The partitioning of the used dataset.

| Data | Normal | COVID-19 | Viral Pneumonia | Overall |
|------|--------|----------|-----------------|---------|
| Training | 700 | 700 | 700 | 2100 |
| Testing | 300 | 300 | 300 | 900 |
| Overall | 1000 | 1000 | 1000 | 3000 |

operation on the patch and kernel values, the kernel generates a single item in the feature map. The patch selection is then moved to the right or below, depending on stride movement. This step is repeated until the entire picture is complete; during training, the kernel values change with each iteration. The aim is to find the optimal kernel weights to assist the model in achieving maximum accuracy while minimizing optimization loss. As a result, different characteristics such as edges, shape, texture and colour-related features are learned.

### *Functions of activation*

A node's capacity for activation or responsiveness cannot be predicted in advance. The use of activation can be used to infer this. To do this, it connects the node's various weights and biases applies the relationship to the node as a function and generate results. It also helps in
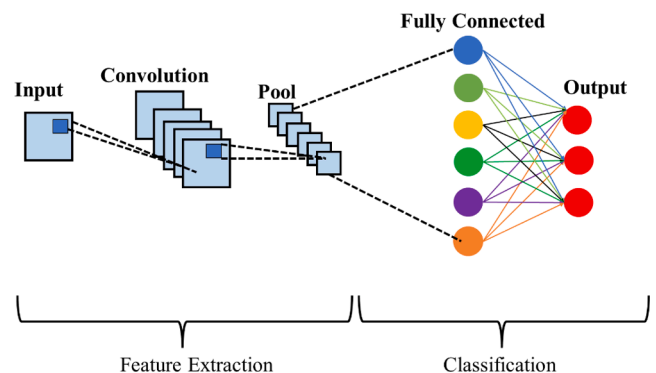


**Fig. 5.** Schematic of Convolutional Neural Network (CNN).

comprehending more complex data patterns. They transform the receiving signals from the node into an output signal that is used as the output or in the next layer of the network. The several activation methods are shown in Table 3 below.

When examining ReLu, the possibility of a vanishing gradient is less

**Table 3**
Activation Function.

| Activation Function | Mathematical Representation | Brief Description |
|---|---|---|
| Binary Step | $(x) = \begin{cases} 0; for\, x < 0 \\ 1; for\, x \geq 0 \end{cases}$ | 1 or 0 |
| Linear | $y(x) = x$ | Linear over $-\infty$ to $\infty$. |
| ReLu (Rectified Linear Unit) | $f(x) = max(0,x)$ | Range [0 to $\infty$) |
| Sigmoid/Logistic | $y(x) = \dfrac{1}{1 + e^{-x}}$ | Range (0, 1) |
| tanh/Hyperbolic | $y(x) = \dfrac{sinh\,x}{cosh\,x}$ | Range ($-1$, 1) |
| Softmax | $softmax(z_i) = \dfrac{exp(z_i)}{\sum_j exp(z_i)}$ | Range (0, 1) and sum of O/Ps = 1 |
| Leaky ReLu | $f(x) = max(0.01*x, x)$ | Range ($-\infty$, $\infty$). |

likely, in contrast to the gradient of sigmoids, which decreases as the absolute value of x increases. We used Relu as the activation function is CNN layers.

*Pooling*

In a CNN, the pooling layers reduce the number of features by down sampling a given input dimension. Some of the suggested pooling layers are Max-pooling, Average-pooling, and Sum-pooling. On the other hand, max-pooling, which is often used for dimensionality reduction, showed great performance. Max-pooling chooses the matrix's greatest value while disregarding all other values. The Max-pooling mathematical equation is shown as:

$$maxpool_{ij} = \max_{p} f'(x)_{i+p,j+p} \tag{1}$$

where i and j present the spatial position.

*Fully connected layer*

Based on characteristics from the convolutional and pooling layers, the FC layer classifies data. A popular activation function in deep learning is SoftMax activation for multi-class classification problems. The SoftMax function's mathematical equation is shown in Table 3. The output of the *kth* convolutional layer can be represented as a 3D tensor $F_k$ with dimensions $W_k$x$H_k$x$C_k$, where $W_k$, $H_k$, and $C_k$ are the width, height, and number of channels of the feature map produced by the *k-th* convolutional layer, respectively. The output of the first convolutional layer is given by:

$$F_k = ReLU(W_k * X + b_k) \tag{2}$$

where $W_k$ is the weight tensor of the first convolutional layer, $b_k$ is the bias tensor, and ReLU is the rectified linear unit activation function. The output of the remaining convolutional layers can be obtained in a similar manner.

*DWT as reduction of feature vector dimension*

The wavelet-transform method was suggested by Grossmann and Morlet (Grossmann & Morlet, 1984). Wavelets are thought of as waves with a finite duration that come in a variety of sizes and shapes. They can be evaluated in both time and frequency. The existence of a large variety of wavelets is the primary strength of wavelet analysis. The scaling component of the wavelet transform, which has two primary components and is inversely proportional to frequency, describes the expansion or compression of the signal in the time domain. Stretched wavelets can describe gradual variations in an image, while shrunken wavelets can indicate rapid changes in the image. Shifting, which indicates the signal's lag or advance, is the second crucial component of the wavelet transform. To align the feature of the signal, a wavelet transform is shifted.

In this work, the sum of wavelets at different time scales and shifts may be used to describe wavelet analysis for CNN vectors using DWT. By separating the temporal and scale components of feature vectors, DWT
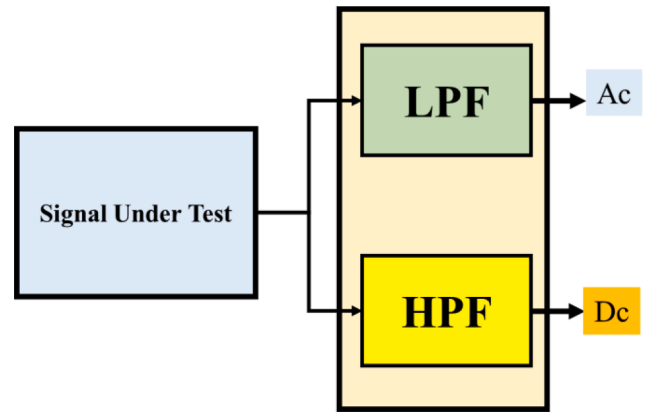


**Fig. 6.** Schematic of DWT showing low pass filter (LPF) and high pass filter (HPF) to get approximation coefficients (Ac) and detail coefficients (Dc).

can extract local features. Approximations and details are two elements of wavelet analysis. Two sets of coefficients are produced by one-dimensional DWT: approximation coefficients (Ac) and detail co-efficients (Dc) (see Fig. 6).

Convoluting the signals with a low-pass filter for approximation and a high-pass filter for accuracy yields these coefficients. The convolved coefficients are down sampled by maintaining the even indexed elements. The sign's identity is determined by its Ac, which is the most important part of the sign. The Dc includes identification data. e.g. The sound of a human speaking signal change when the Dc is removed, yet it is still comprehensible. This becomes incoherent when the Ac information is removed. As a result, Ac is used in DWT analysis.

The second DWT is applied to the Ac component from the first DWT process in two-dimensional DWT, resulting in new Ac and Dc values. Since one-dimensional DWT was used in this investigation, the first Ac component of the signal was acquired. We used 1-D DWT to extract the detail coefficients from each vector. In this work, the feature vector produced by CNN was coupled with 1-D DWT to enhance the classification performance of LSTM. The objective is that by doing so, the feature vector's dimension will be lowered but important characteristics of the feature vector will be kept. In summary, DWT transforms the feature vector into a further elaborated, reduced, and strengthened signal and detect signal discontinuities. The feature vectors of images that were obtained from CNN were decomposed into low-frequency components with 1-D DWT and then trained with LSTM network to classify.

The feature vectors obtained from the last convolutional layer are decomposed using 1D DWT. Let *V* be the input feature vector of length *N*, and let *Ac* and *Dc* be the approximation and detail coefficients obtained from the 1D DWT, respectively. Then the decomposition can be expressed as:

$$V = A_c + D_c \tag{3}$$

The DWT operates on each feature map $f_i$ separately and extracts local features by separating the temporal and scale components of the feature vectors. For each feature map $f_i$, we compute the one-dimensional DWT as follows:

$$A_c(j,k) = <f_i, \varphi(j,k)> = \sum n f_i(n)\varphi(j,k,n) \tag{4}$$

$$D_c(j,k) = <f_i, \psi(j,k)> = \sum n f_i(n)\psi(j,k,n) \tag{5}$$

where $\varphi(j,k,n)$ and $\psi(j,k,n)$ are the scaling and wavelet functions at scale *j* and position *k*, respectively. The coefficients $A_c(j,k)$ and $D_c(j,k)$ represent the approximate and detail coefficients, respectively, at scale *j* and position *k*. The DWT is applied at different scales and shifts to
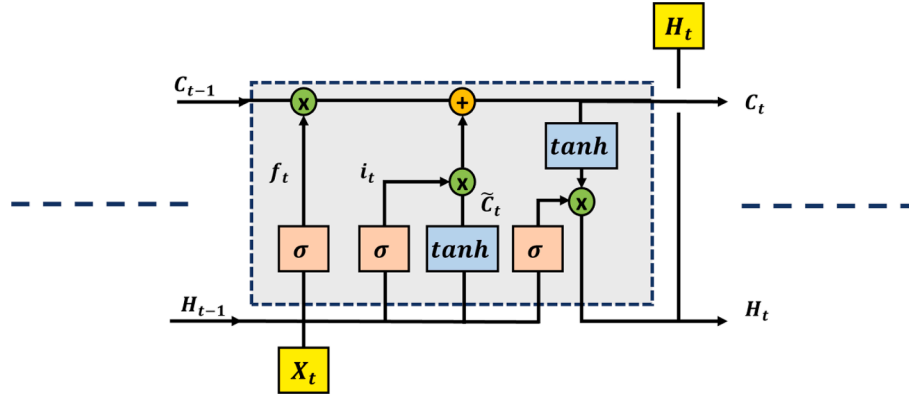
**Fig. 7.** Schematic of the Long short-term memory network.

capture local features at different resolutions. The sum of wavelets at different time scales and shifts is used to describe wavelet analysis for CNN vectors.

### Long short-term memory model

CNN processes network input data in unconnected segments. When it comes to connected data, such as time series, this method only works for uncorrelated data. Utilizing correlated input data in the form of a time series, recurrent neural networks were developed (RNNs). The LSTM design was developed to address the RNNs' long-term memory problem (Schmidhuber & Hochreiter, 1997). To avoid the long-term vanishing gradient problem, LSTM models were utilised. Similarly, in the context of temporal feature detection, LSTMs can be used to identify and extract relevant features processing the data in a sequential manner and learning temporal patterns. This can be particularly useful when dealing with complex, multi-dimensional data where the temporal relationships between features are important, such as in medical signal analysis as used in this work. The operating concept of the LSTM architecture is shown in Fig. 7. The four gates of the LSTM architecture are the input gate, forget gate, update gate, and output gate, each of which represents an artificial neural network. The length of the input sequence is indicated by the t-time in the mathematical equations for these gates in Eqs. (6)–(9). To put it another way, t-time is the LSTM's time step. The duration of the DWT output is referred to as t-time in this study. The following diagrams depict the LSTM input gate's concept.

$$i_t = \sigma(W_i*[h_{t-1}, x_t] + b_i) \tag{6}$$

$$\widetilde{C}_t = tanh(W_i*[h_{t-1}, x_t] + b_i) \tag{7}$$

$$C_t = f_T C_{t-1} + i_t \widetilde{C}_t \tag{8}$$

$$f_t = \sigma(W_f*[h_{t-1}, x_t] + b_f) \tag{9}$$

where (2) is utilised to select which chunk of information should be included by passing $h_{t-1}$ and $x_t$ through a sigmoid layer. After $h_{t-1}$ and $x_t$ have been transferred through the tanh layer, (3) is used to get fresh information.

In (4), the present moment information, $\widetilde{C}_t$, and longterm memory information, $C_{t-1}$, are integrated, where $W_i$ denotes a sigmoid output and $\widetilde{C}_t$ denotes a tanh output. $W_i$ stands for weight matrices, while $b_i$ - stands for the LSTM's input gate bias. The forget gate of the LSTM

allows for the selective transfer of information using a sigmoid layer and a dot product. Eq. (5) is used to decide whether to forget relevant information from a previous cell with a particular probability, where $W_f$ denotes the weight matrix, $b_f$ the offset and $\sigma$ is the sigmoid function.

Following (6) and (7), the LSTM's output gate determines the states that are necessary for the $h_{t-1}$ and $x_t$ inputs to continue (7). The state decision vectors that carry fresh information, $C_t$ via the *tanh* layer are multiplied by the final output.

$$O_t = \sigma(W_o*[h_{t-1}, x_t] + b_o) \tag{10}$$

$$h_t = O_t tanh(C_t) \tag{11}$$

where $W_o$ and $b_o$ are the weighted matrices and LSTM bias of the output gate, respectively.

### Combined CNN-DWT-LSTM network

Using three different types of X-ray images, a combination approach was created to automatically detect COVID-19 instances in this study. This architecture's structure was created by integrating CNN, DWT and LSTM networks, with the CNN extracting complicated spatial information from pictures and DWT reducing the dimension of the feature vector and the LSTM acting as a classifier. The suggested hybrid network for COVID-19 detection is shown in Fig. 8. There are 21 layers in the network: twelve convolutional layers, six pooling layers, one FC layer, one LSTM layer, and one softmax output layer. Each convolution block is made up of two or three CNNs and one pooling layer, followed by a dropout layer with a 35% L1 regularization preventing overfitting. The ReLU function activates the convolutional layer. To minimize the dimensions of a feature map, the max-pooling layer with a size of $2 \times 2$ kernels is utilized. The feature vectors of images that were obtained from CNN were decomposed into low-frequency components with 1-D DWT and then trained with LSTM network to classify. The output shape is discovered to be after the convolutional block (none, 8, 8, 512). The LSTM layer's input size has been reduced using the reshape approach (64, 512). Table 4 shows an overview of the planned architecture. The proposed design can classify the X-ray images through a completely connected layer after assessing the features to forecast whether they belong to COVID-19, viral pneumonia, or normal. In order to make this clearer, we have added the pseudocode 1 to explain the overall sequence of the process.

**Pseudocode 1: CORONA-NET Architecture**

**Initialize** the parameters (image)

for 1: MaxIter

***do***

  *for* data input

    ***CNN***

    **Generate** a feature map by performing convolution on input image using a kernel.

    **Reduce** the dimension of the feature map using max or average pooling operation.

    **Repeat** steps a-b with different kernels to extract different features.

    **Pass** the output of the last convolutional layer through a fully connected layer with Softmax activation to classify data.

    ***DWT***

    **Apply** 1D DWT to extract the detail coefficients from each CNN feature vector.

    **Combine** the resulting coefficients to obtain a new, lower-dimensional feature vector.

    ***LSTM***

    **Pass** the feature vector obtained from 1D DWT through LSTM to extract temporal features.

    **Output** of the last LSTM cell is used as input to the dense layer.

    ***Dense Layer***

    **Apply** Softmax activation to the output of the last LSTM cell to obtain class probabilities.

    **Highest** probability class is chosen as the predicted class label.

    **Return Output**: Class label

| Layers | Type | Stride | Kernel | Kernel Size | Input Size |
|--------|------|--------|--------|-------------|------------|
| 1 | Convolution | 1 | 64 | 3 x 3 | 256 x 256 x 3 |
| 2 | Convolution | 1 | 64 | 3 x 3 | 256 x 256 x 64 |
| 3 | Pool | 2 | - | 2 x 2 | 256 x 256 x 64 |
| 4 | Convolution | 1 | 128 | 3 x 3 | 128 x 128 x 64 |

***Performance metrics***

The performance metrics for the proposed system are defined below. TP (true positive) indicates correctly predicted COVID-19 instances, FP (false positive) indicates normal, or pneumonia cases misclassified as COVID-19 by the proposed method, TN (true negative) indicates correctly classified normal or pneumonia cases and FN (false negative) indicates COVID-19 cases misclassified as normal or pneumonia cases by the proposed system. FP represents the number of sequence points when the electrical appliance is running but the result is non-functional. The electrical appliance is not in use, but the model decomposition result is, as shown by the number FN, which stands for the total number of sequence points. $Y_t$ at time t represents the actual power of the electrical apparatus. The average absolute error of the power disaggregation from time $T_0$ to time $T_1$ is known as MAE. The disaggregated power at time t is represented by the variable $y_t$, and MAE is the average absolute error of the power disaggregation across the time range $T_0$–$T_1$. The non-intrusive load disaggregation basic indicators of PRE, REC, and F1 scores may be used to gauge how accurately the model determines if an electrical appliance is in a working condition.

$$Sensitivity = \frac{TP}{TP + FN}$$

$$Specificity = \frac{TN}{TN + FP}$$

$$Accuracy = \frac{TP + TN}{TN + FP + TP + FN}$$

$$F1 - score = \frac{2*TP}{2*TP + FP + FN}$$

## 6. Results and discussion

***Simulation setup***

We divided the dataset into training, validation and testing in this study, with 70, 15 and 15 percent going to each. Fig. 8 depicts the proposed COVID-19 detecting combinational network. The network has 21 layers: 12 convolutional layers, 6 pooling layers, 1 FC layer, 1 LSTM layer, and 1 softmax output layer. Each convolution block consists of two or three 2D CNNs, one pooling layer, and a dropout layer with a 35 percent L1 regularisation to avoid overshooting. Python 3.10.0 was used and) all of the models were built using the Keras package and TensorFlow 2.7.0. We utilised a Graphic Processor Unit (GPU) with 130 GB of RAM. Batch size of 16 was used with Adaptive Moment Estimation (ADAM) as an optimizer and learning rate of 0.1 was employed.

***Results analysis***

Fig. 9 depicts the CORONA-NET architecture's confusion matrix for the COVID-19 sickness categorization. One instance of viral pneumonia was misclassified as a normal patient among the 900 images, two viral pneumonia patients were misclassified as COVID-19, and one COVID-19 patient was misclassified as a viral pneumonia patient. The suggested network outperforms competing proposed networks because it has more reliable true positive and true negative values than the others, as well as less false negative and false positive values. The recommended approach may thus classify COVID-19 instances with accuracy.

The CORONA-NET training and validation phases are graphically depicted in terms of accuracy and cross-entropy (loss) in the Fig. 10. At
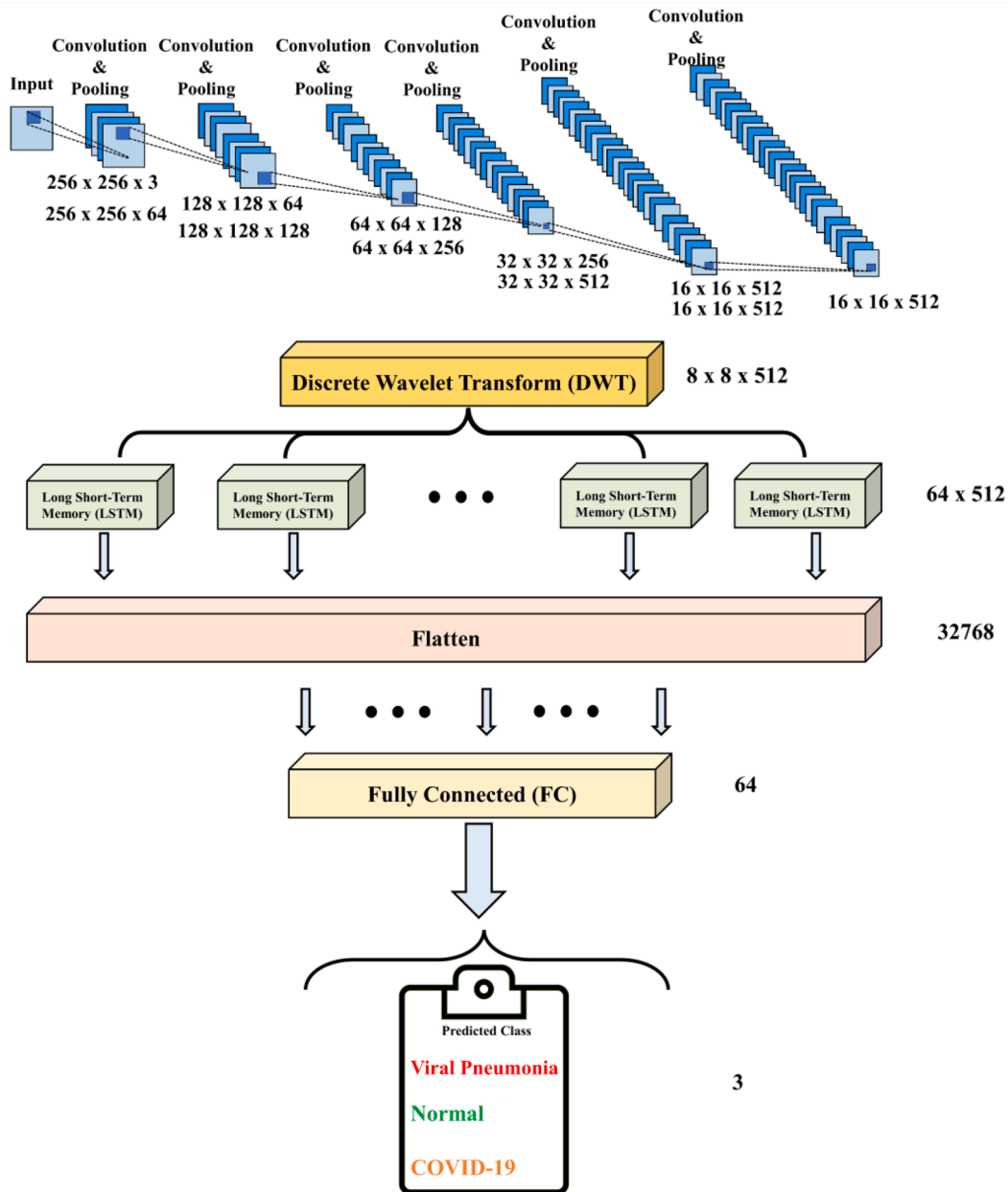
**Fig. 8.** Schematic of the proposed CORONA-Net detection.

epoch 125, the acquired training and validation accuracy are 99.2 percent and 98.1 percent, respectively. Similarly, the CORONA-NET design has training and validation losses of 0.04 and 0.05, respectively.

Table 5 display the CORONA-NET network's performance characteristics for each class. The COVID-19 category was recognised with outstanding accuracies, specificities, sensitivity, precision, and F1-score (99.556, 99.667, 99.667, 99.336 and 99.501 percent). The specificity value (99.667 percent) shows that the total amount of true negatives is high while the sensitivity value (99.667 percent) shows that the total amount of false negatives is low. For the categorization of pneumonia, it had 99.556, 99.833, 99, 99.664 and 99.331 percent accuracy, specificity, sensitivity, and F1-score. For the healthy patients, it had accuracy, specificity, sensitivity, precision, and F1-score of 99.556, 99.833, 100, 99.668, and 99.834 percent. While the normal people had the maximum sensitivity and F1-score, pneumonia sufferers had lower sensitivity scores.

The results of the proposed system are compared with the recent articles in the Table 6 on the similar data set that are used in the

comparative works (Bell, Murphy, & Moreira, 2023; S.I. di Radiologia Medical interventistica, 2021; Paul Mooney 2021; NIH Kaggle, 2021). It is clear that the proposed architecture has a very good presentation but also has a very less computational overheads that makes this detection a feasible method.

There are various drawbacks to the suggested system. To begin with, the sample size needs to be enlarged in order to evaluate the generalizability of the constructed system. Second, it only looks at the posterior anterior (PA) perspective of X-rays, thus it can't tell the difference between other X-ray views like anterior posterior (AP), lateral, and so on.

***Ablation study***

In order to check and justify proposed network, we conducted an ablation study on the backbone CNN feature extractor, Discrete Wavelet Transform (DWT) (feature detctor) block, and LSTM (temporal feature detector) block. We evaluate the efficacy of the model where we remove these components out of the network and compare the performance with that of the complete network. From the Table 7, it is clear that the combination of these three models together integrated as CORONA-NET

**Table 4**
Summary of CORONA-NET Architecture.

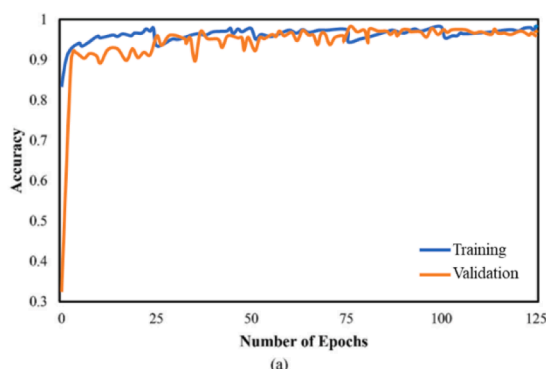| Layers | Type | Stride | Kernel | Kernel Size | Input Size |
|---|---|---|---|---|---|
| 1 | Convolution | 1 | 64 | 3 × 3 | 256 × 256 × 3 |
| 2 | Convolution | 1 | 64 | 3 × 3 | 256 × 256 × 64 |
| 3 | Pool | 2 | – | 2 × 2 | 256 × 256 × 64 |
| 4 | Convolution | 1 | 128 | 3 × 3 | 128 × 128 × 64 |
| 5 | Convolution | 1 | 128 | 3 × 3 | 128 × 128 × 128 |
| 6 | Pool | 2 | – | 2 × 2 | 128 × 128 × 128 |
| 7 | Convolution | 1 | 256 | 3 × 3 | 64 × 64 × 128 |
| 8 | Convolution | 1 | 256 | 3 × 3 | 64 × 64 × 256 |
| 9 | Pool | 2 | – | 2 × 2 | 64 × 64 × 256 |
| 10 | Convolution | 1 | 512 | 3 × 3 | 32 × 32 × 256 |
| 11 | Convolution | 1 | 512 | 3 × 3 | 32 × 32 × 512 |
| 12 | Pool | 2 | – | 2 × 2 | 32 × 32 × 512 |
| 13 | Convolution | 1 | 512 | 3 × 3 | 32 × 32 × 512 |
| 14 | Convolution | 1 | 512 | 3 × 3 | 16 × 16 × 512 |
| 15 | Pool | 2 | – | 2 × 2 | 16 × 16 × 512 |
| 16 | Convolution | 1 | 512 | 3 × 3 | 16 × 16 × 512 |
| 17 | Convolution | 1 | 512 | 3 × 3 | 16 × 16 × 512 |
| 18 | Pool | 2 | – | 2 × 2 | 16 × 16 × 512 |
| DWT | | | | | |
| 19 | LSTM | – | – | – | 64 × 512 |
| 20 | FC | – | 64 | – | 32,768 |
| 21 | Output | – | 3 | – | 64 |
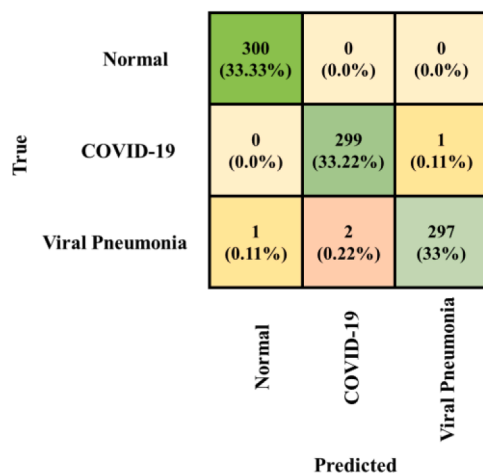


**Fig. 9.** Confusion Matrix.

results in the highest accuracy.

## 7. Technique validation

Understanding the COVID-19 detection cycle or map in the hospital as opposed to the cycle of activities needed in the indicated detection is vital to establish the validity analysis of the data obtained. Fig. 11 (a) shows the standard technique to COVID-19 detection whereas Fig. 11 (b) shows the recommended methodology's process flow for early COVID-19 detection. This research comprised COVID-19 individuals who presented to the hospital with respiratory complaints. The cases considered for the study were those in whom the virus caused pneumonia and radiographic abnormalities were discovered on chest x-rays and CBCT scans.

For the validation of the results obtained, it is important to benchmark the detection method with the observation findings of the radiologist to see if the detection has been accurate or not and PCR test done at day 1, 3 and 5. For this purpose, we have taken the diagnosis of the radiologist consultant and Professor of Radiology (Dr. Ayesha Ahmed) and Professor of Medicine from AH, Denmark if the cases were declared as a COVID-19 positive, normal or viral pneumonia as compared to CORONA-NET detection results. We have selected 25 patients for this purpose. The cases considered for the study were those in which the virus caused pneumonia and radiographic abnormalities were discovered on chest x-rays and CBCT scans. The results of the PCR tests conducted on days 1, 3, and 5 are shown in Table 8, together with the results of the suggested procedure. All of the patients in this sample area are those who were identified as suspects with COVID in the outpatient department (OPD). The findings produced using the traditional methods lead to erroneous and incorrect detection, which can happen at the following four stages:

- GP stage: Based on symptoms, an Outpatient Department (OPD) may refer a patient for further PCR and a chest x-ray in order to rule out COVID-19.
- The radiologist errs and overlooks the COVID-19.
- Despite the symptoms and the X-ray both clearly indicating COVID-19, the PCR test is negative on day 1 (the day of the report).
- The PCR test is negative on day 3, but the chest X-ray indicates COVID-19.

The results shown in Table 9 validate that there has never been a false detection with the proposed technique, however, there is the process flow available if a patient tests COVID-19 positive on the third day.

## 8. Limitations and future work

COVID-19 detection using X-ray images with CORONA-NET has the following disadvantages, including:

Limited sensitivity: Chest X-rays can miss up to 30% of COVID-19 cases, especially in the early stages of infection when symptoms may be mild or absent. This limited sensitivity of X-ray images makes the use of this technique limited due to X-ray images sensitivity.
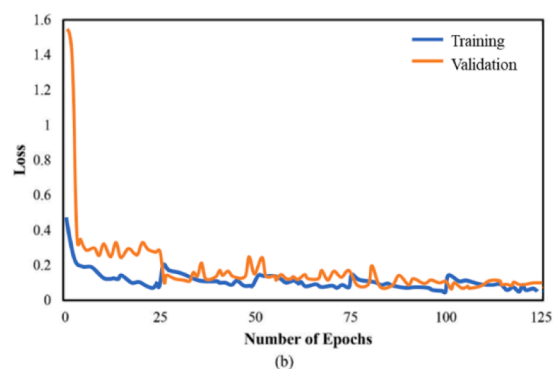


**Fig. 10.** Evaluation of CORONA-NET architecture for COVID-19 in terms of (a) Accuracy (b) Loss.

**Table 5**

Performance of the CORONA-NET Architecture.

| Class | Accuracy (%) | Specificity (%) | Sensitivity (%) | Precision (%) | F1-score (%) |
|---|---|---|---|---|---|
| Normal | 99.556 | 99.833 | 100 | 99.668 | 99.834 |
| COVID-19 | 99.556 | 99.667 | 99.667 | 99.336 | 99.501 |
| Viral Pneumonia | 99.556 | 99.833 | 99 | 99.664 | 99.331 |

**Table 6**

Performance of the CORONA-NET Architecture.

| Author | Model | Accuracy (COVID-19) (%) | Training (min) | Testing (min) |
|---|---|---|---|---|
| Loey et al. (2020) | GoogleNet | 81 | – | – |
| Ucar and Korkmaz (2020) | COVIDiagnosis-Net | 98.3 | 40 | – |
| Apostolopoulos and Mpesiana (2020) | VGG19 | 93.5 | – | – |
| Maghdid et al. (2021) | Xception | 89.5 | – | – |
| Sethy and Behera (2020) | SVM | 95.4 | – | – |
| El Asnaoui and Chawki (2021) | Inception | 92.2 | 1319.4 | 4.4 |
| Li, Li, and Zhu (2020) | DenseNet | 88.9 | – | – |
| Chowdhury, Rahman, Khandakar, Mazhar, Kadir, Mahbub, and Al-Emadi (2020) | SGDM-SqueezeNet | 98.3 | – | – |
| Farooq and Hafeez (2020) | ResNet50 | 96.2 | – | – |
| Hemdan, Shouman, and Karar (2020) | VGG19 | 90 | 44.016 | 0.067 |
| Rahimzadeh and Attar (2020) | ResNet50 | 91.4 | – | – |
| Islam, Islam, and Asraf (2020) | CNN | 98 | 306.2 | 1.88 |
| Proposed Method | CORONA-NET | 99.566 | 67 | 12 |

**Table 7**

Performance of the CORONA-NET Architecture.

| Model | Accuracy (COVID-19) (%) |
|---|---|
| CNN | 89% |
| CNN-DWT | 94.3% |
| LSTM (alone) | 87% |
| CNN-LSTM | 91% |
| LSTM-DWT | 94% |
| CORONA-NET | 99.566 |

Lack of specificity: X-rays can show abnormal lung findings that are not specific to COVID-19, making it difficult to distinguish COVID-19 from other respiratory diseases.

Radiation exposure: Repeated exposure to X-rays can increase the risk of cancer and other health problems over time, particularly in younger patients.

Dependence on expertise: Accurate interpretation of X-rays requires specialized training and experience, which may not be available in all healthcare settings.

Cost and accessibility: X-ray machines are expensive and may not be available in some resource-limited settings, making it difficult to use X-rays as a routine screening tool for COVID-19.

Overall, while chest X-rays can provide useful information in diagnosing COVID-19, they should not be used as the sole diagnostic tool, and other tests such as PCR or antigen tests should be used for confirmation. Similarly, the CNN-DWT-LSTM model has shown great promise for COVID detection using X-ray data, and there is still much to be done to further improve its accuracy and effectiveness. The future works will consdier the following points:

Data augmentation: It is important to increase the amount of training data to improve the performance of the CNN-DWT-LSTM model. This can be achieved through various data augmentation techniques such as flipping, rotation, scaling, and adding noise to the X-ray images. Transfer learning: Transfer learning is a technique that involves leveraging pre-trained models to improve the performance of a new model. In the case of COVID detection using X-ray data, a pre-trained CNN model such as VGG or ResNet can be used as a starting point to train the CNN-DWT-LSTM model.

Fusion of different modalities: While X-ray data is useful for COVID detection, other imaging modalities such as CT scans and MRI can provide complementary information. Therefore, a future work can be done to investigate the fusion of different modalities to improve the accuracy of the CNN-DWT-LSTM model.

Explainability: CNN-DWT-LSTM model is a deep learning model which is known for being a "black box" model, which means that it can be difficult to interpret its decision-making process. Therefore, developing an explainable AI technique that can provide insights into the features and patterns used by the model to make its predictions can be a valuable future work.

Multi-task learning: Multi-task learning involves training a single model to perform multiple related tasks. In the context of COVID detection using X-ray data, multi-task learning can be applied to simultaneously predict COVID-19 infection and the severity of the disease.

Real-time prediction: Currently, the CNN-DWT-LSTM model requires processing time for making predictions. Therefore, a future work can be done to develop a real-time prediction system that can make quick and accurate predictions of COVID-19 infection from X-ray data.

## 9. Summary

The increase in COVID-19 is rising every day while the detection of a single positive case is significant to reduce the spread. For the identification of COVID-19 from X-ray images, we developed a CNN-DWT-LSTM-based CORONA-NET architecture. For the identification of coronavirus, CORONA-NET is employed for the feature extraction and classification. The proposed system has a 99.56 percent accuracy, 99.667 percent specificity, 99.667 percent sensitivity, 99.336 percent precision and 99.501 percent F1 score suggesting that the proposed design outperforms the competing networks. It is expected that in the midst of the worldwide COVID-19 pandemic, the suggested system would be able to perform robust COVID-19 detection and minimize the workload of COVID-19 medical diagnosis. To make our suggested model more robust, we will investigate and include a varied data set with more COVID-19 instances in future work. The concept of the suggested design is not without flaws. The use of limited data sets is the key flaw. As a result, we plan to perform additional trials in the future by collecting more data sets and collaborating with radiologists to improve our model's accuracy.

**CRediT authorship contribution statement**

**Muhammad Usman Hadi:** Conceptualization, Methodology, Software, Supervision, Data curation, Investigation, Project administration, Resources, Validation, Writing - original draft, Writing - review & editing. **Rizwan Qureshi:** Data curation, Investigation, Writing - original draft, Writing - review & editing. **Ayesha Ahmed:** Visualization,
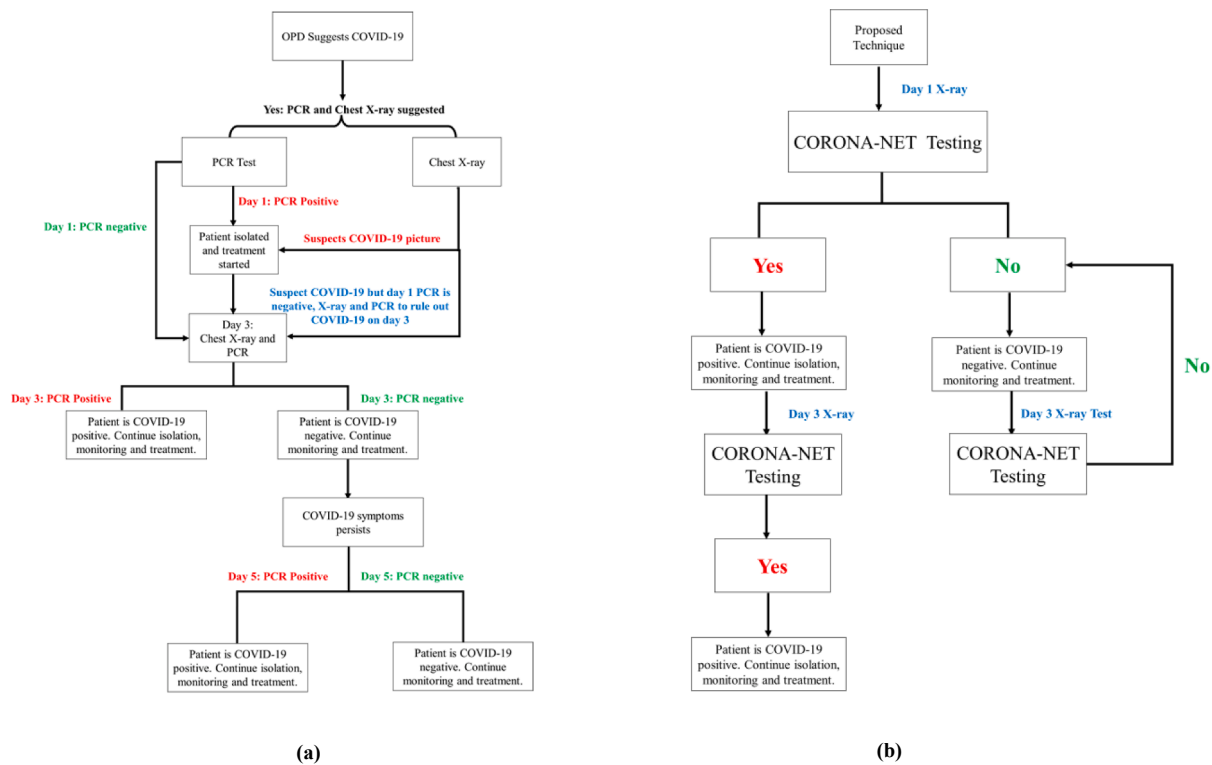
**Fig. 11.** (a) Process flow for the hospital's observational early identification of COVID-19 using PCR and X-ray (b) Process flow for the hospital's observational traditional COVID-19 detection (PCR and X-ray).

**Table 8**
Collected data for 25 samples with Radiologist findings, Results of PCR on days 1 (day of observation), 3, and 5 using the method we suggested.

| Sample # | PCR Test Day 1 | Radiologist Findings | PCR Test Day 3 | PCR Test Day 5 | Proposed Technique Test Day 1 |
|---|---|---|---|---|---|
| 1 | Positive | COVID-19 | Positive | Positive | Positive |
| 2 | Negative | COVID-19 | Positive | Positive | Positive |
| 3 | Negative | COVID-19 | Positive | Positive | Positive |
| 4 | Positive | COVID-19 | Positive | Positive | Positive |
| 5 | Positive | COVID-19 | Positive | Positive | Positive |
| 6 | Negative | COVID-19 | Positive | Positive | Positive |
| 7 | Negative | Pneumonia | Negative | Negative | Negative |
| 8 | Positive | COVID-19 | Positive | Positive | Positive |
| 9 | Negative | Pneumonia | Negative | Negative | Negative |
| 10 | Positive | COVID-19 | Positive | Positive | Positive |
| 11 | Negative | Pertussis | Negative | Negative | Negative |
| 12 | Negative | Pneumonia | Negative | Negative | Negative |
| 13 | Negative | COVID-19 | Positive | Positive | COVID-19 |
| 14 | Negative | Pneumonia | Negative | Negative | No |
| 15 | Positive | COVID-19 | Positive | Positive | Positive |
| 16 | Positive | COVID-19 | Positive | Positive | Positive |
| 17 | Negative | COVID-19 | Negative | Positive | Positive |
| 18 | Positive | COVID-19 | Positive | Positive | Positive |
| 19 | Negative | COVID-19 | Positive | Positive | Positive |
| 20 | Negative | COVID-19 | Positive | Positive | Positive |
| 21 | Negative | Pneumonia | Positive | Positive | Positive |
| 22 | Positive | COVID-19 | Positive | Positive | Positive |
| 23 | Positive | COVID-19 | Positive | Positive | Positive |
| 24 | Negative | COVID-19 | Positive | Positive | Positive |
| 25 | Negative | COVID-19 | Negative | Positive | Positive |

**Table 9**
Statistical evaluation of existing and suggested false detection techniques.

| Specification | Value |
|---|---|
| Total Number of Samples | 25 |
| PCR Test Day 1 Missed Detection | 10 |
| X-rays synopsis Missed Detection | 1 |
| PCR Test Day 3 Missed Detection | 2 |
| PCR Test Day 5 Missed Detection | 0 |
| Proposed Technique Test Day 1 Missed Detection | 0 |

interests or personal relationships that could have appeared to influence the work reported in this paper.

**Data availability**

Data will be made available on request.

Investigation. **Nadeem Iftikhar:** Software, Validation, Writing – review & editing.

**Declaration of Competing Interest**

The authors declare that they have no known competing financial

**References**

Alzubaidi, L., Zhang, J., Humaidi, A. J., Al-Dujaili, A., Duan, Y., Al-Shamma, O., … Farhan, L. (2021). Review of deep learning: Concepts, CNN architectures, challenges, applications, future directions. *Journal of Big Data, 8*, 1–74.

Antiochia, R. (2020). Nanobiosensors as new diagnostic tools for SARS, MERS and COVID-19: From past to perspectives. *Microchimica Acta, 187*, 1–13.

Apostolopoulos, I. D., & Mpesiana, T. A. (2020). Covid-19: Automatic detection from x-ray images utilizing transfer learning with convolutional neural networks. *Physical and Engineering Sciences in Medicine, 43*, 635–640.

Baltruschat, I. M., Nickisch, H., Grass, M., Knopp, T., & Saalbach, A. (2019). Comparison of deep learning approaches for multi-label chest X-ray classification. *Scientific Reports, 9*(1), 1–10.

Bell, D., Murphy, A., Moreira, M. COVID-19. Reference article, *Radiopaedia.org* (Accessed on 28 Mar 2023). https://doi.org/10.53347/rID-73913.

Cai, X. F., Chen, J., Hu, J. L., Long, Q. X., Deng, H. J., Liu, P., … Wang, D. Q. (2020). A peptide-based magnetic chemiluminescence enzyme immunoassay for serological diagnosis of coronavirus disease 2019. *The Journal of Infectious Diseases, 222*(2), 189–193.

Chen, X., Tang, Y., Mo, Y., Li, S., Lin, D., Yang, Z., … Dai, Z. (2020). A diagnostic model for coronavirus disease 2019 (COVID-19) based on radiological semantic and clinical features: A multi-center study. *European Radiology, 30*, 4893–4902.

Cho, S. I., Sun, S., Mun, J. H., Kim, C., Kim, S. Y., Cho, S., … Chung, J. H. (2020). Dermatologist-level classification of malignant lip diseases using a deep convolutional neural network. *British Journal of Dermatology, 182*(6), 1388–1394.

Chowdhury, M. E. H., Rahman, T., Khandakar, A., Mazhar, R., Kadir, M. A., Mahbub, Z. B., ... & Al-Emadi, N. Can AI help in screening viral and COVID-19 pneumonia? 2020, ArXiv Prepr. arXiv preprint ArXiv:2003.13145.

Civit-Masot, J., Luna-Perejón, F., Domínguez Morales, M., & Civit, A. (2020). Deep learning system for COVID-19 diagnosis aid using X-ray pulmonary images. *Applied Sciences, 10*(13), 4640.

Clark, K., Vendt, B., Smith, K., Freymann, J., Kirby, J., Koppel, P., … Prior, F. (2013). The Cancer Imaging Archive (TCIA): Maintaining and operating a public information repository. *Journal of Digital Imaging, 26*, 1045–1057.

El Asnaoui, K., & Chawki, Y. (2021). Using X-ray images and deep learning for automated detection of coronavirus disease. *Journal of Biomolecular Structure and Dynamics, 39*(10), 3615–3626.

Farooq, M., & Hafeez, A. (2020). Covid-resnet: A deep learning framework for screening of covid19 from radiographs. arXiv preprint arXiv:2003.14395.

Feng, W., Newbigging, A. M., Le, C., Pang, B., Peng, H., Cao, Y., … Le, X. C. (2020). Molecular diagnosis of COVID-19: Challenges and research needs. *Analytical chemistry, 92*(15), 10196–10209.

Giri, B., Pandey, S., Shrestha, R., Pokharel, K., Ligler, F. S., & Neupane, B. B. (2021). Review of analytical performance of COVID-19 detection methods. *Analytical and bioanalytical chemistry, 413*(1), 35–48.

Grossmann, A., & Morlet, J. (1984). Decomposition of Hardy functions into square integrable wavelets of constant shape. *SIAM Journal on Mathematical Analysis, 15*(4), 723–736.

Hashmi, M. F., Katiyar, S., Keskar, A. G., Bokde, N. D., & Geem, Z. W. (2020). Efficient pneumonia detection in chest xray images using deep transfer learning. *Diagnostics, 10*(6), 417.

Hemdan, E. E. D., Shouman, M. A., & Karar, M. E. (2020). Covidx-net: A framework of deep learning classifiers to diagnose covid-19 in x-ray images. arXiv preprint arXiv:2003.11055.

Islam, M. Z., Islam, M. M., & Asraf, A. (2020). A combined deep CNN-LSTM network for the detection of novel coronavirus (COVID-19) using X-ray images. *Informatics in Medicine Unlocked, 20*, Article 100412.

Jung, C., Levy, C., Varon, E., Biscardi, S., Batard, C., Wollner, A., … Cohen, R. (2021). Diagnostic accuracy of SARS-CoV-2 antigen detection test in children: A real-life study. *Frontiers in Pediatrics, 9*, Article 647274.

Kakodkar, P., Kaka, N., & Baig, M. N. (2020). A comprehensive literature review on the clinical presentation, and management of the pandemic coronavirus disease 2019 (COVID-19). *Cureus, 12*(4).

Kallianos, K., Mongan, J., Antani, S., Henry, T., Taylor, A., Abuya, J., & Kohli, M. (2019). How far have we come? Artificial intelligence for chest radiograph interpretation. *Clinical Radiology, 74*(5), 338–345.

Khatri, A., Jain, R., Vashista, H., Mittal, N., Ranjan, P., & Janardhanan, R. (2020). Pneumonia identification in chest X-ray images using EMD. In Trends in Communication, Cloud, and Big Data: Proceedings of 3rd National Conference on CCB, 2018 (pp. 87–98). Springer Singapore.

Lee, G., & Fujita, H. (Eds.). (2020). *Deep learning in medical image analysis: challenges and applications* (Vol. 1213). Springer Nature.

Li, X., Li, C., & Zhu, D. (2020). Covid-mobilexpert: On-device covid-19 screening using snapshots of chest x-ray.

Loey, M., Smarandache, F., & Khalifa, N. E. M. (2020). Within the lack of chest COVID-19 X-ray dataset: A novel detection model based on GAN and deep transfer learning. *Symmetry, 12*(4), 651.

Maghdid, H. S., Asaad, A. T., Ghafoor, K. Z., Sadiq, A. S., Mirjalili, S., & Khan, M. K. (2021). Diagnosing COVID-19 pneumonia from X-ray and CT images using deep learning and transfer learning algorithms. In *Multimodal image exploitation and learning 2021* (Vol. 11734, pp. 99–110). SPIE.

Mooney, Paul (2018). Chest X-ray images (pneumonia) | Kaggle. *Kaggle.com.* https://www.kaggle.com/paultimothymooney/chest-xray.

Mousavizadeh, L., & Ghasemi, S. (2021). Genotype and phenotype of COVID-19: Their roles in pathogenesis. *Journal of Microbiology, Immunology and Infection, 54*(2), 159–163.

Nasrullah, N., Sang, J., Alam, M. S., Mateen, M., Cai, B., & Hu, H. (2019). Automated lung nodule detection and classification using deep learning combined with multiple strategies. *Sensors, 19*(17), 3722.

Nguyen, V., Cai, J., & Chu, J. (2019). August). Hybrid CNN-GRU model for high efficient handwritten digit recognition. In *Proceedings of the 2nd international conference on artificial intelligence and pattern recognition* (pp. 66–71).

Nguyen, T., Duong Bang, D., & Wolff, A. (2020). 2019 novel coronavirus disease (COVID-19): Paving the road for rapid detection and point-of-care diagnostics. *Micromachines, 11*(3), 306.

NIH chest X-rays | Kaggle. https://www.kaggle.com/nih-chest-xrays/data?select=Data_Entry_2017.csv. [Accessed 29 Oct 2021].

Oberfeld, B., Achanta, A., Carpenter, K., Chen, P., Gilette, N. M., Langat, P., … Pillai, S. (2020). SnapShot: Covid-19. *Cell, 181*(4), 954.

Ozturk, T., Talo, M., Yildirim, E. A., Baloglu, U. B., Yildirim, O., & Acharya, U. R. (2020). Automated detection of COVID-19 cases using deep neural networks with X-ray images. *Computers in Biology and Medicine, 121*, Article 103792.

Passaro, V. M., de Tullio, C., Troia, B., La Notte, M., Giannoccaro, G., & De Leonardis, F. (2012). Recent advances in integrated photonic sensors. *Sensors, 12*(11), 15558–15598.

Rahimzadeh, M., & Attar, A. (2020). A modified deep convolutional neural network for detecting COVID-19 and pneumonia from chest X-ray images based on the concatenation of Xception and ResNet50V2. *Informatics in Medicine Unlocked, 19*, Article 100360.

S.I. di Radiologia Medical interventistica, Covid-19 database. https://www.sirm.org/en/category/articles/covid-19-database/.

Sahajpal, N. S., Mondal, A. K., Njau, A., Ananth, S., Jones, K., Ahluwalia, P. K., … Kota, V. (2020). Proposal of RT-PCR–based mass population screening for severe acute respiratory syndrome coronavirus 2 (coronavirus disease 2019). *The Journal of Molecular Diagnostics, 22*(10), 1294–1299.

Schmidhuber, J., & Hochreiter, S. (1997). Long short-term memory. *Neural Computation, 9*(8), 1735–1780.

Schuit, E., Veldhuijzen, I. K., Venekamp, R. P., Van den Bijllaardt, W., Pas, S. D., Lodder, E. B., … Moons, K. G. (2021). Diagnostic accuracy of rapid antigen tests in asymptomatic and presymptomatic close contacts of individuals with confirmed SARS-CoV-2 infection: Cross sectional study. *BMJ, 374*.

Sethy, P. K., & Behera, S. K. (2020). Detection of coronavirus disease (covid-19) based on deep features.

Sharma, M., & Miglani, N. (2020). Automated brain tumor segmentation in MRI images using deep learning: Overview, challenges and future. *Deep Learning Techniques for Biomedical and Health Informatics, 347–383*.

Sisti, N., Valente, S., Mandoli, G. E., Santoro, C., Sciaccaluga, C., Franchi, F., … Cameli, M. (2021). COVID-19 in patients with heart failure: The new and the old epidemic. *Postgraduate Medical Journal, 97*(1145), 175–179.

Son, J., Shin, J. Y., Kim, H. D., Jung, K. H., Park, K. H., & Park, S. J. (2020). Development and validation of deep learning models for screening multiple abnormal findings in retinal fundus images. *Ophthalmology, 127*(1), 85–94.

Stephen, O., Sain, M., Maduh, U. J., & Jeong, D. U. (2019). An efficient deep learning approach to pneumonia classification in healthcare. *Journal of Healthcare Engineering.*

Taha, B. A., Al Mashhadany, Y., Hafiz Mokhtar, M. H., Dzulkefly Bin Zan, M. S., & Arsad, N. (2020). An analysis review of detection coronavirus disease 2019 (COVID-19) based on biosensor application. *Sensors, 20*(23), 6764.

Ucar, F., & Korkmaz, D. (2020). COVIDiagnosis-Net: Deep Bayes-SqueezeNet based diagnosis of the coronavirus disease 2019 (COVID-19) from X-ray images. *Medical Hypotheses, 140*, Article 109761.

Vandenberg, O., Martiny, D., Rochas, O., van Belkum, A., & Kozlakidis, Z. (2021). Considerations for diagnostic COVID-19 tests. *Nature Reviews Microbiology, 19*(3), 171–183.

Wang, Y., Wang, C., & Zhang, H. (2018). Ship classification in high-resolution SAR images using deep learning of small datasets. *Sensors, 18*(9), 2929.

World Health Organization. (2021). *The impact of COVID-19 on health and care workers: A closer look at deaths (No. WHO/HWF/WorkingPaper/2021.1)*. World Health Organization.

Worldometer COVID-19 Coronavirus Pandemic. https://www.worldometers.info/coronavirus/.

Yang, M., Li, H., Sun, J., Zhao, Y., & Tang, D. (2020). Focus on Characteristics of COVID-19 with the Special Reference to the Impact of COVID-19 on the Urogenital System. *Current Urology, 14*(2), 79–84.

Yao, L., Poblenz, E., Dagunts, D., Covington, B., Bernard, D., & Lyman, K. (2017). Learning to diagnose from scratch by exploiting dependencies among labels. arXiv preprint arXiv:1710.10501.

Zhang, Y., Wang, G., Li, M., & Han, S. (2018). Automated classification analysis of geological structures based on images data and deep learning model. *Applied Sciences, 8*(12), 2493.

Zhu, N., Zhang, D., Wang, W., Li, X., Yang, B., Song, J., ... & Tan, W. (2020). A novel coronavirus from patients with pneumonia in China, 2019. *New England Journal of Medicine.*